NANO LETTERS

Letter

pubs.acs.org/NanoLett

Effect of Atomic Interconnects on Percolation in Single-Walled Carbon Nanotube Thin Film Networks

Xiaojuan Tian,[†,§] Matthew L. Moser,[‡,§] Aron Pekker,[‡,§] Santanu Sarkar,[‡,§] Jason Ramirez,[†,§] Elena Bekyarova,[‡,§] Mikhail E. Itkis,[‡,§] and Robert C. Haddon*[,†,‡,§,¶]

[†]Department of Chemical Engineering, University of California, Riverside, California 92521, United States

[‡]Department of Chemistry, University of California, Riverside, California 92521, United States

[§]Center for Nanoscale Science and Engineering, University of California, Riverside, California 92521, United States

[¶]Department of Physics, King Abdulaziz University, Jeddah 21589, Saudi Arabia

S *Supporting Information*

ABSTRACT: The formation of covalent bonds to single-walled carbon nanotube (SWNT) or graphene surfaces usually leads to a decrease in the electrical conductivity and mobility as a result of the structural rehybridization of the functionalized carbon atoms from sp^2 to sp^3. In the present study, we explore the effect of metal deposition on semiconducting (SC-) and metallic (MT-) SWNT thin films in the vicinity of the percolation threshold and we are able to clearly delineate the effects of weak physisorption, ionic chemisorption with charge transfer, and covalent hexahapto (η^6) chemisorption on these percolating networks. The results support the idea that for those metals capable of forming bis-hexahapto-bonds, the generation of covalent (η^6-SWNT)M(η^6-SWNT) interconnects provides a conducting pathway in the SWNT films and establishes the transition metal bis-hexahapto organometallic bond as an electronically conjugating linkage between graphene surfaces.

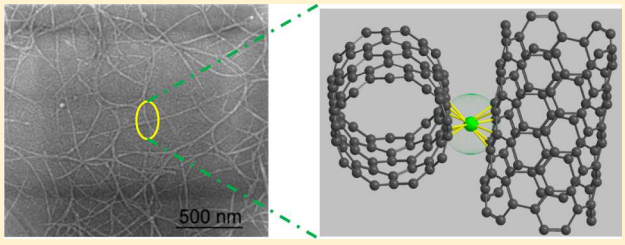

KEYWORDS: *Organometallic hexahapto bonds, carbon contacts, graphene, atomtronics*

The interaction of metals with the benzenoid surfaces of carbon nanotubes and graphene can significantly modify their electronic and magnetic structure and plays an important role in the realization of electrical contacts to carbon-based electronic devices.[1] Depending on the nature of the metal atoms, their interaction with graphene surfaces is described by three distinct behaviors: (a) weak physisorption, (b) chemisorption with ionic character (doping) and little rehybridization, and (c) chemisorption with covalent bonding, in which there is minimal charge transfer but strong rehybridization of the carbon atoms from sp^2 to sp^3.[2,3] We refer to this third category as destructive rehybridization as it usually leads to a loss of conductivity and a reduction in mobility of the graphene nanostructures. Recently, we suggested a fourth category: (d) chemisorption in which the covalent interaction leads to the formation of an electronically conjugating, organometallic bis-hexahapto-graphene junction while maintaining the electronic structure of the individual graphene nanostructures; such bonds involve minimal (structural) rehybridization and we have referred to this process as constructive rehybridization.[4]

The extended, periodic π-electron graphitic structures are narrow or zero band gap materials and, thus, the electron-donor and electron-acceptor interactions between the highest occupied molecular orbitals (HOMOs) and lowest unoccupied molecular orbitals (LUMOs) of the arene π-system, and the d-orbitals of transition metals in hexahapto-metal bonds, are strongly enhanced by the high lying valence band and low lying conduction band of the graphitic surfaces.[4,5] In analogy with benzene, in which the e_{1g} and e_{2u} π-orbitals hybridize with the metal d-orbitals to form the hexahapto-metal-bonds in (η^6-benzene)$_2$Cr, the electronic structure of the graphitic π-electron systems is ideally suited for the realization of organometallic chemistry.[4−7]

As we show below, single walled carbon nanotube (SWNT) networks offer a unique platform to study the effect of the hexahapto-metal bond on the establishment of electrical contact between graphitic surfaces. The electrical resistance of thin films of SWNTs is known to be dominated by the internanotube junctions,[8] as confirmed in conductive tip atomic force microscopy[9−12] and cross junction electrical resistance studies.[13,14] Because the current flows easily along the nanotubes before being forced to surmount the internanotube junction resistance, it is apparent that the percolation in these films is dominated by the nature of the internanotube contacts. Thus, we reasoned that the transport in such SWNT films—particularly in the vicinity of the percolation threshold—would be particularly sensitive to the formation of (η^6-SWNT)M(η^6-SWNT) interconnects because in this regime the conducting

Received: April 1, 2014
Revised: May 20, 2014
Published: June 3, 2014

 © 2014 American Chemical Society dx.doi.org/10.1021/nl501212u | *Nano Lett.* 2014, 14, 3930−3937

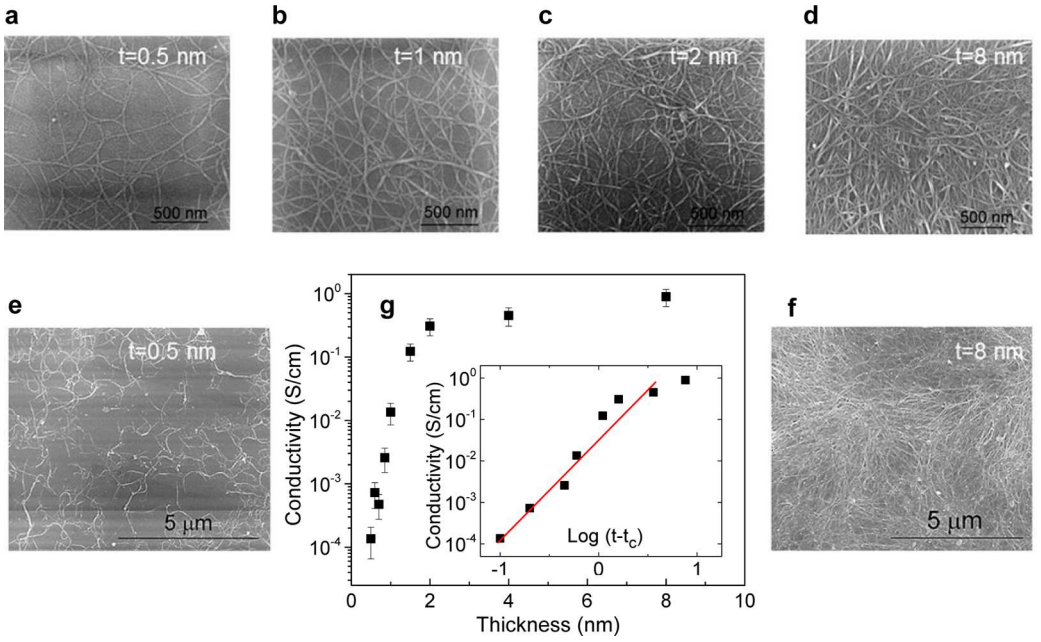

Figure 1. SEM images of SC-SWNT films of thicknesses (a, e) 0.5 nm; (b) 1 nm; (c) 2 nm; and (d, f) 8 nm. (g) Room temperature conductivity of pristine SC-SWNT films as a function of effective thickness. Inset of (g) shows a fit of conductivity data to eq 1 with parameters $t_c \sim 0.4$ nm and $\alpha = 2.4$.

pathways become severely limited by the low density of SWNTs. The use of transition metals to interconnect SWNT surfaces represents the first attempt to use covalent bonding to modulate the conductivity of SWNT thin film networks; prior to this work, the covalent functionalization of graphene and SWNT surfaces have led to a decrease in the conductivity and mobility.[15,16] Previous approaches to improve the conductivity of SWNT thin film networks have relied on an increase in the carrier concentration by use of electrochemical and solid state gating or by exposure to dopants, which lead to ionic charge transfer chemistry, and thus, we rely on this latter technique to benchmark our use of hexahapto-metal SWNT interconnects.

The SWNT networks are of interest in their own right and have been shown to provide a readily accessible platform for device applications, including their use as diodes and transistors,[17,18] chemical and biosensors,[19−21] and near-IR detectors.[22−24] The p-type semiconducting behavior of the SWNT thin films in conjunction with their optical transparency makes them suitable for transparent conductive coatings in large area solar cells, light emitting diodes and displays,[8,17,25−30] and as reconfigurable optical media.[31]

In the present manuscript we report the effect of the deposition of suitably chosen metals on the conductivities of metallic (MT-) and semiconducting (SC-) SWNT films of nominal thickness (t), t = 0.5, 1, 2, 4, 8 nm. As we show below, these thicknesses approach the critical thickness (t_c) for percolation and offer an ideal platform with which to benchmark the ability of the covalent (η^6-SWNT)M(η^6-SWNT) bond to enhance the connectivity of a SWNT network. We chose metals to represent three of the limiting cases discussed above: (a) physisorption (gold), (b) chemisorption with ionic doping (lithium), and (d) chemisorption with bis-hexahapto-bonding (constructive rehybridization, chromium).[4,32] The experiments follow the e-beam version of the metal vapor synthesis (MVS) technique, which has proved to be very successful in the low temperature preparation of many bis-hexahapto-metal complexes,[33−35] although our substrates are held near room temperature.

Transport Properties of Pristine Semiconducting Single-Walled Carbon Nanotube (SC-SWNT) Thin Films. The SWNT films were prepared from aqueous dispersions of SC- and MT-SWNTs by filtration and the effective thickness (t) of the film was calculated from the mass of the dispersed SWNTs and the measured film density of 1.2 g/cm^3;[32] during film formation the individual SWNTs reassemble into bundles of diameter 3−6 nm. The SEM images in Figure 1 show the emergence of network inhomogeneities in the thinnest films as evidenced by the appearance of spatial fluctuations in the density of SWNTs and is readily observed by comparing the uniformity of the films of effective thickness 0.5 nm (Figure 1a,e) and 8 nm (Figure 1d,f), in agreement with literature reports.[28,36,37]

The pristine films were annealed at 300 °C for 3 h in a vacuum of 10^{-7} Torr before transfer to the vacuum system where they were further annealed at 110 °C to minimize atmospheric p-type doping;[38] the electrical conductivities were measured in a 2-probe configuration as 4-probe measurements showed a negligible contribution of the current contacts to the film resistance. The conductivity of the pristine SC-SWNT films at 300 K as a function of thickness is shown in Figure 1g; the film of thickness t = 0.5 nm has a measured resistance of $R = 4 \times 10^{11}$ ohm and a conductivity $\sigma = 8 \times 10^{-5}$ S/cm. The conductivity of the pristine SC-SWNT films shows a pronounced increase between t = 0.5 and 2 nm, beyond which it saturates at a bulk conductivity, $\sigma \sim 1$ S/cm.

The strong dependence of conductivity on film thickness agrees with expectations based on percolation theory[39,40] and as shown in Figure 1g (inset) can be satisfactorily described by the expression

$$\sigma \propto (t - t_c)^{\alpha} \quad (1)$$

with an estimated percolation threshold, $t_c \sim 0.4$ nm for the SC-SWNT films and critical exponent $\alpha = 2.4$, in good

dx.doi.org/10.1021/nl501212u | Nano Lett. 2014, 14, 3930−3937

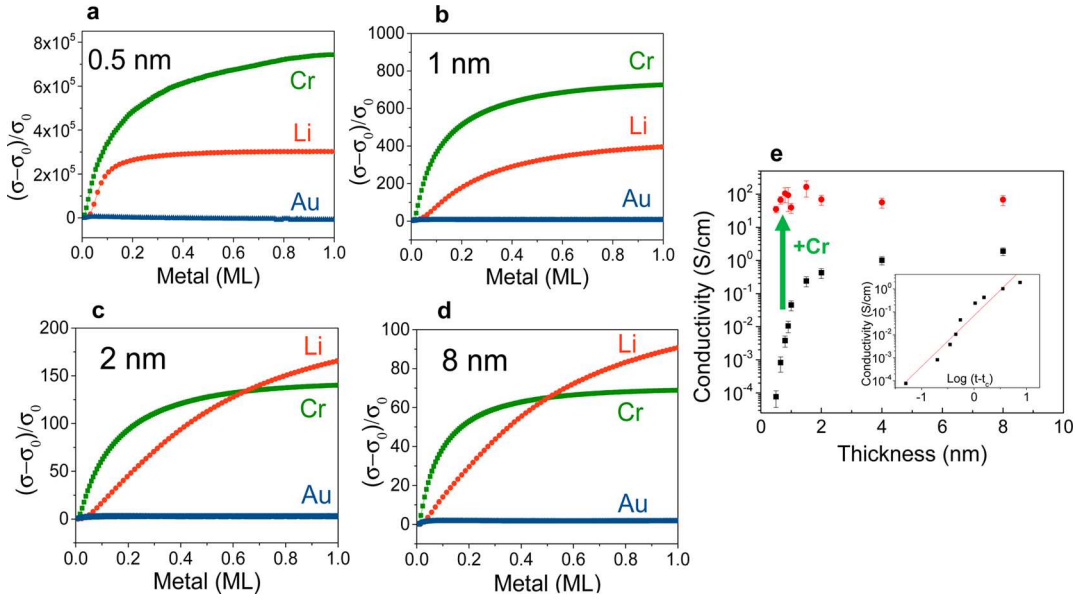

Figure 2. Effect of metal deposition on the electrical conductivity of SC-SWNT films of thicknesses: (a) 0.5 nm; (b) 1 nm; (c) 2 nm; and (d) 8 nm. (e) Conductivities of SC-SWNT films before (black square symbols) and after (red circle symbol) 0.1 ML Cr deposition. Inset of (e) shows a fit of the conductivity data to eq 1 with parameters $t_c \sim 0.45$ nm and $\alpha = 2.2$.

agreement with the value of $t_c = 1-3$ nm previously obtained for thin films of nonseparated SWNTs.[28,41,42] In order to test the reproducibility of the data, a second set of independently prepared SWNT films was evaluated and found to give similar results ($t_c \sim 0.45$ nm and $\alpha = 2.2$).

The critical thickness obtained from the percolation analysis is subject to two extrinsic factors: (a) the tendency of the SWNTs to rebundle during film preparation, thereby reducing the number of conducting pathways available for electrical transport and (b) the inhomogeneity of the SWNT network in very thin films, which requires the percolating pathways to include the sparsely covered areas surrounding high density islands (Figure 1e). The values of α obtained in this study exceed the universal critical exponents for 2D and 3D percolating systems of 1.33 and 1.94,[39] although critical exponents above the universal values were previously reported for SWNT networks[28,42,43] and composite system[40] and predicted theoretically for systems with a wide distribution of bond or junction resistances.[40,44,45]

Metal Deposition on SC-SWNT Thin Films. Below, we explore the use of metals in improving internanotube junction resistance and we report the results of high vacuum metal deposition experiments conducted on ultrathin SWNT networks in the vicinity of the percolating threshold. Prior to metal deposition the SWNT films were annealed and then transferred into a cryopumped Temescal BJD 1800 e-beam evaporator equipped with custom fittings to allow in situ measurement of the film resistance.

The behavior of the SC-SWNT conductivity on the deposition of one monolayer (ML) of metal is shown in Figure 2 as a function of the SWNT film thickness. The SC-SWNT thin films show a strong increase in conductivity on deposition of alkali and transition metals, whereas the deposition of gold leads to a very small, monotonic increase in conductivity (not visible in Figure 2), which is consistent with the formation of a parallel noninteracting film due to the fact that gold is unable to participate in bis-hexahapto-bonding owing to its filled outer d-orbital [physisorption, case a].[4]

The deposition of lithium is expected to result in charge transfer to the SWNTs [case b above, ionic chemisorption, doping], and alkali metals are known to produce a strong increase in the conductivity of carbon nanomaterials.[46−48]

Recently, we found that Cr can form (η^6-SWNT)M(η^6-SWNT) interconnects,[32,49] and we have suggested that this mode of interaction with the graphene surfaces of carbon nanomaterials is totally distinct from ionic chemisorption and physisorption. The formation of (η^6-SWNT)Cr(η^6-SWNT) complexes is particularly favorable (Figure 3) because the

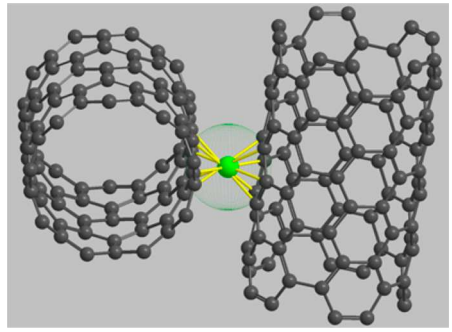

Figure 3. Bis-hexahapto bond formation at the internanotube junctions.

distance between the benzene rings in the prototypical bis(benzene)chromium complex, $(\eta^6\text{-}C_6H_6)_2Cr$ (3.23 Å),[50] is close to the van der Waals gap of 3.15 Å within SWNT bundles.[51] The 6 valence electrons from the Cr atom in conjugation with two Clar sextets from the graphene surface[4] of the SWNTs lead to a total of 18 electrons, which exactly fill the 3d4s4p metal valence shell, and it is known to lead to a stable electronic configuration.[32,52]

Reference to Figure 2 shows that in the initial stage of metal deposition ($t_M < 0.5$ ML) on SC-SWNT films, the conductivity enhancement induced by the Cr atoms is more efficient than the doping by Li, and thus, at very low coverage, the ability of

dx.doi.org/10.1021/nl501212u | Nano Lett. 2014, 14, 3930−3937

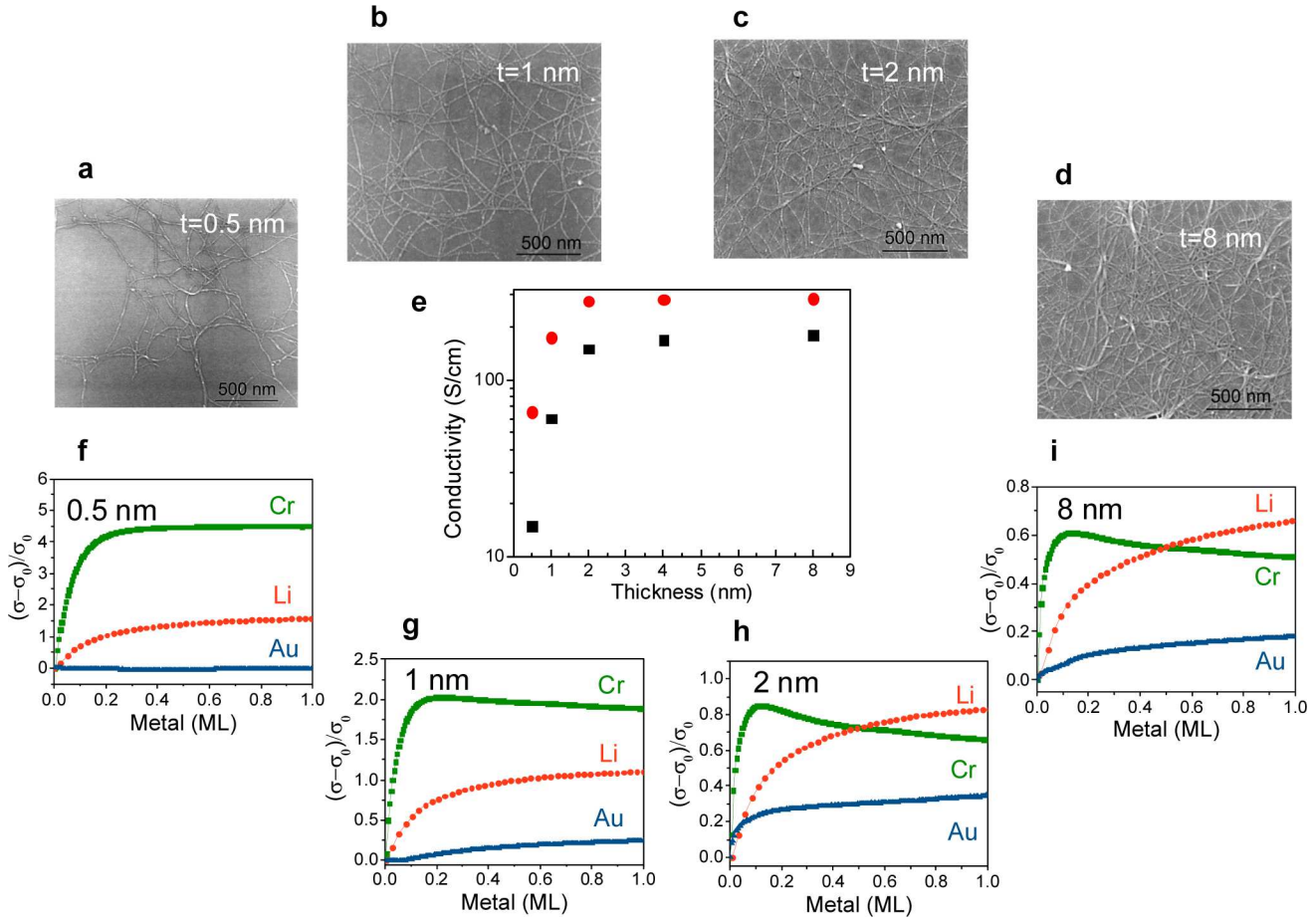

Figure 4. SEM images of MT-SWNTs films of thicknesses: (a) 0.5 nm; (b) 1 nm; (c) 2 nm; and (d) 8 nm. (e) Percolating dependence of conductivities of MT-SWNT films before (black) and after (red) 0.1 ML Cr deposition. Effect of metal deposition on electrical conductivity of MT-SWNTs films (f–i) of thicknesses: (f) 0.5 nm; (g) 1 nm; (h) 2 nm, and (i) 8 nm.

Cr to bridge the highly resistive SWNT contacts is always more effective than electron transfer via doping to the conduction band of SC-SWNTs. Beyond this point, we distinguish between two cases: pristine SC-SWNT films that have reached the saturation conductivity (Figure 2, $t_{SWNT} \geq 2$ nm), and pristine SC-SWNT films below this thickness (which are approaching t_c: $t_{SWNT} \leq 1$ nm). For those pristine SC-SWNT thin films beyond the saturation conductivity ($t_{SWNT} \geq 2$ nm), Li doping eventually becomes more effective in its ability to enhance the bulk SC-SWNT film conductivity. In the situation where the SC-SWNT film approaches the percolation threshold ($t_{SWNT} \leq 1$ nm), it may be seen that Cr is always more effective than Li in enhancing the conductivity of the SC-SWNT network, and this is in accord with a situation in which the conductivity is severely limited by the number of conducting pathways. At these thicknesses, the SC-SWNT film conductivities are extremely dependent on the quality of the network junctions and the conductivity enhancements by the Cr atoms are about a factor of 700 (t = 1 nm) and 700 000 (t = 0.5 nm), clearly indicating that these films are in the vicinity of the critical thickness for percolation (t_c). In such sparse inhomogeneous networks, the establishment of a few SWNT electrical interconnects by bis-hexahapto-bond formation can dramatically increase the conductance of the film (Figure 2a). After Cr deposition, all of the SC-SWNT film conductivities are found to be independent of thickness, which suggests that the formation of (η^6-SWNT)Cr(η^6-SWNT) bonds is able to completely remedy the weak links in the SWNT network to the point that percolation effects are no longer apparent in the data (Figure 2e).

Metal Deposition on MT-SWNT Thin Films. SEM images of networks of MT-SWNTs of effective thicknesses 0.5–8 nm are presented in Figure 4a–d together with the dependence of the electrical conductivity on the film thickness, which indicates a percolation threshold below a film thickness of 0.5 nm.

For the thinnest measured MT-SWNT film (t = 0.5 nm), the room temperature resistance was $R = 2.3 \times 10^6$ ohm (σ = 15 S/cm), which is 5 orders of magnitude lower than the value measured for a SC-SWNT film of the same thickness (above). Despite this difference in the film resistances, the saturation values of the conductivities occur in the same range of thicknesses (2–8 nm) for SC- and MT-SWNTs; this result emphasizes the importance of the density of physical SWNT junctions in these films and number of conducting pathways rather than the absolute conductivities.

The behavior of the MT-SWNTs film conductivities on the deposition of gold (Figure 4) is similar to that seen for the SC-SWNTs, although this change is not visible in the results shown in Figure 2. With a few caveats, the qualitative features of the response of the MT-SWNT films to the deposition of Li and Cr resemble that of the SC-SWNT films, although the magnitude of the response is 2 to 4 orders of magnitude less. In all cases, the deposition of about 0.1 ML Cr leads to an abrupt increase in the conductivity of the MT-SWNT films; for the pristine

dx.doi.org/10.1021/nl501212u | Nano Lett. 2014, 14, 3930–3937

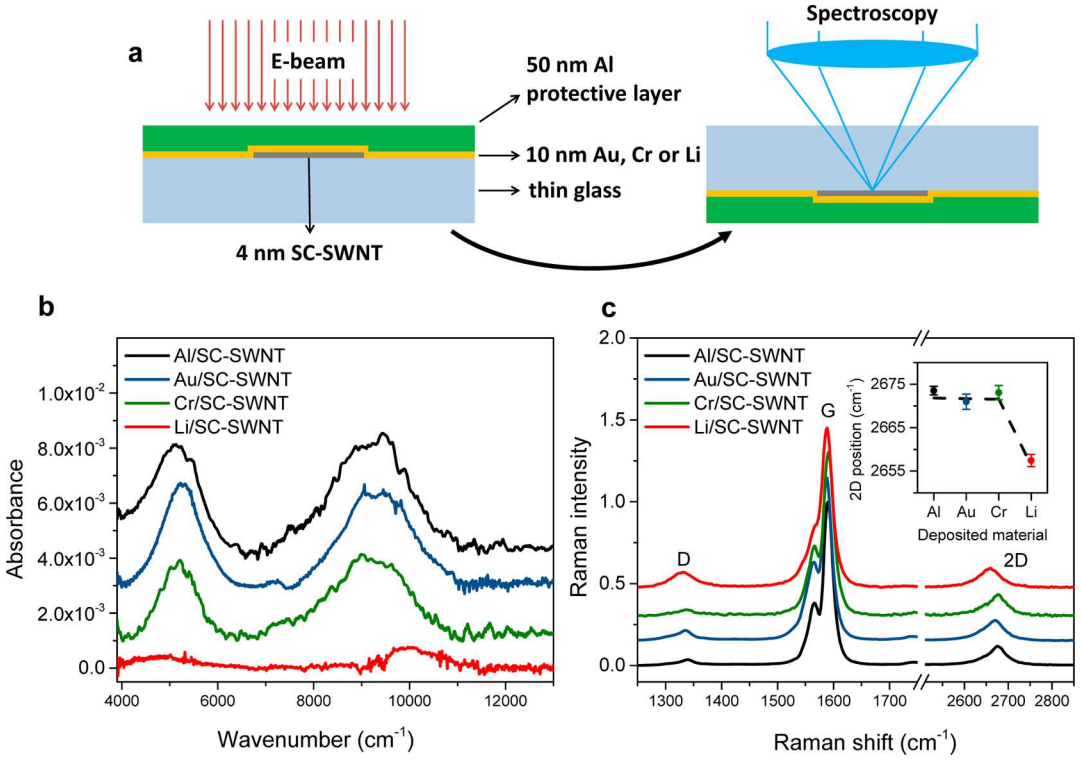

Figure 5. Absorption and Raman spectroscopy of 4 nm thick SC-SWNT films after metal deposition. (a) Sample preparation and experimental configuration for metal deposition (left) and microspectroscopy (right). (b) SWNT thin film near-infrared absorption spectra after aluminum (black curve), gold (blue curve), chromium (green curve) and lithium (red curve) deposition. The spectra were background corrected and vertically offset for clarity. (c) SWNT Raman spectra after aluminum (black), gold (blue), chromium (green), and lithium (red) deposition. The spectra were normalized and vertically offset for clarity. The inset shows a plot of the 2D peak positions of the samples.

films, which have reached the saturation conductivity (Figure 2a, $t_{SWNT} \geq 2$ nm), Li doping becomes more effective in its ability to enhance the MT-SWNT film conductivity at $t_M >$ ~0.5 ML. For the pristine MT-SWNT films, which are below the saturation conductivity ($t_{SWNT} \leq 1$ nm), Cr is always more effective than Li in enhancing the conductivity of the SWNT networks. In most of the films shown in Figure 4, it may be seen that Cr metal deposition beyond about 0.1 ML leads to a slow decrease in the film conductivities, which we attribute to hybridization of the Cr atom with the SWNT metallic states along the body of the SWNTs which act to weakly scatter the conduction electrons [chemisorption, case c; destructive rehybridization, see above]. This result emphasizes the very small number of Cr atoms that are actually involved in bridging the SWNT−SWNT junctions and in constructing conducting pathways.

Although the conductivities of the SC-SWNTs (Figure 2a−d) and the MT-SWNTs (Figure 4f−i) differ by many orders of magnitude, their response to ionic doping and to covalent bond formation are identical in the sense that Cr is always more effective below the saturation conductivity of the pristine films (Figure 2a and 4f, $t_{SWNT} \leq 1$ nm). This is to be expected as above this thickness the conductivities of the pristine films are invariant to further increases in thickness because the physical junction density has reached the bulk value.

Spectroscopic Studies of the Metal-SWNT Thin Films. Although we have noted clear distinctions between the three metals measured in our transport studies, both lithium [(b) ionic chemisorption], and chromium [(d) covalent chemisorption with hexahapto bonding] strongly enhance the conductivities of the SC-SWNT networks. However, the degree of charge transfer from the metal to the SWNT conduction band is expected to be quite different for these two bonding configurations, and thus, we performed spectroscopic studies in order to examine the effects of metal deposition on the electronic structure of the SWNTs.

In order to protect the SWNT networks from the atmosphere, the films were encapsulated with an Al film (50 nm, Figure 5a) in the final deposition step to prevent aerial exposure; Figure 5 shows the spectral characteristics of 4 nm thick SC-SWNT films after metal deposition. The characteristic near-infrared absorption bands related to the first (S_{11}) and second (S_{22}) interband transitions of semiconducting nanotubes are visible in both the reference (SC-SWNT/50 nm Al) and the gold and chromium treated (SC-SWNT/10 nm Au/50 nm Al, SC-SWNT/10 nm Cr/50 nm Al) samples.[53] The unperturbed nature of these peaks suggests the preservation of the SWNT intrinsic band electronic structure and band filling, despite the metal deposition. Lithium deposition on the other hand significantly decreases these absorption features by transfer of electrons to the conduction bands of the SC-SWNTs. Thus, as expected, lithium functions as an n-type dopant and shifts the Fermi level of the nanotubes well into the van Hove singularities, which prevents the interband transitions as a result of Pauli blocking.[54]

Raman spectroscopy was carried out on the same set of samples, and the characteristic SWNT features are apparent in the date given in Figure 5c. It is well known that the position of the 2D band is a sensitive indicator of charge transfer to the SWNTs,[55] and it may be seen that there is no change in the peak position of the SC-SWNT/Cr/Al sample, whereas the SC-SWNT/Li/Al sample shows a significant shift of the 2D peak to

dx.doi.org/10.1021/nl501212u | Nano Lett. 2014, 14, 3930−3937

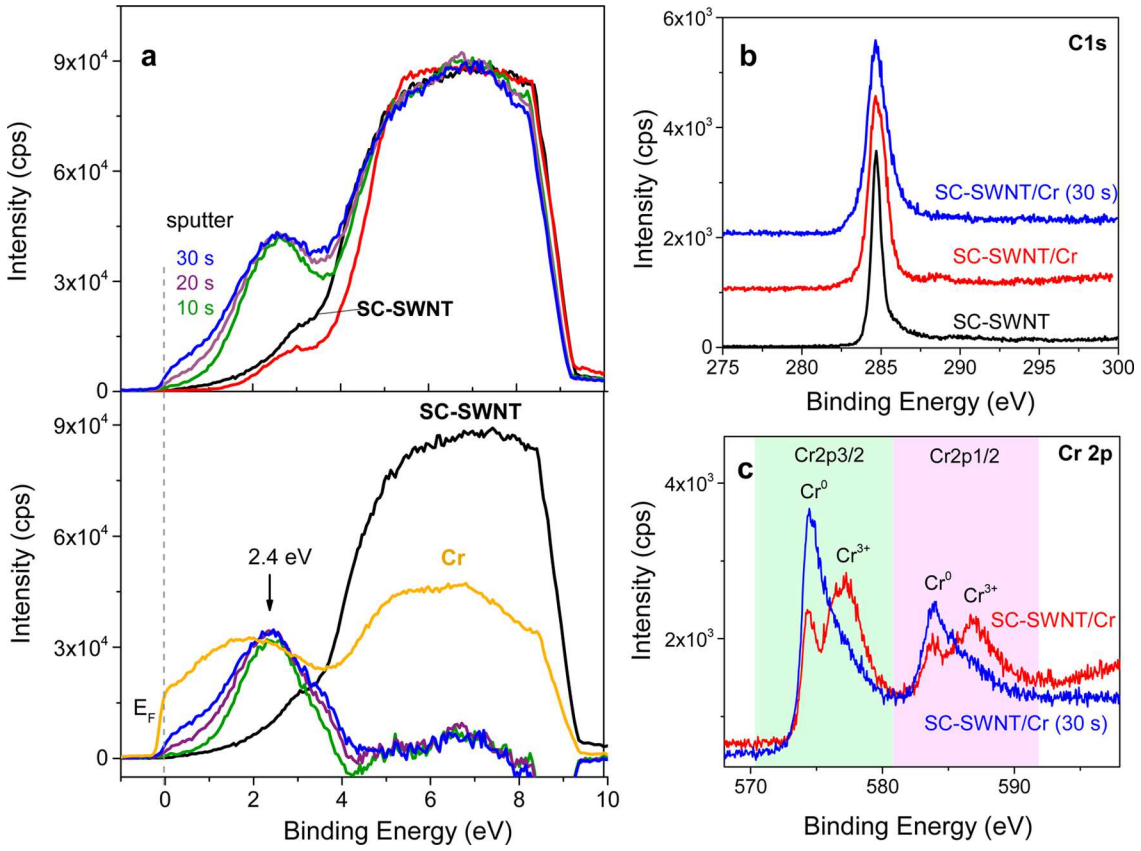

Figure 6. Photoelectron spectra in the ultraviolet (UPS, He I) and X-ray (XPS) regimes for a SC-SWNT film (50 nm film on a HOPG substrate) before and after e-beam deposition of 1 nm Cr. (a) UPS spectra of SC-SWNT (black line), SC-SWNT with 1 nm Cr (SC-SWNT/Cr, red), and SC-SWNT/Cr after sputtering for 10 s (green), 20 s (purple), and 30 s (blue); all spectra are normalized to the 2p-σ transitions at 6–7 eV. The bottom panel shows the difference spectra of the sputtered Cr/SC-SWNT sample obtained after subtraction of the SC-SWNT contribution. (b) Normalized C 1s XPS spectra of SC-SWNT, SC-SWNT/Cr, and 30 s sputtered SC-SWNT/Cr. (c) Cr 2p XPS spectra of SC-SWNT, SC-SWNT/Cr, and 30 s sputtered SC-SWNT/Cr.

lower wavenumbers.[55] On the basis of the spectroscopic data, we conclude that the interaction of Cr atoms with the SWNTs does not induce significant charge transfer, and thus, the bonding is covalent rather than ionic in nature, as discussed above.

The effect of chromium on the electronic structure of SC-SWNTs was further examined with ultraviolet photoelectron spectroscopy (UPS) and Figure 6a shows the valence band spectra of a SC-SWNT film before and after the deposition of 1 nm Cr. The spectrum of pristine SC-SWNTs is very similar to that of HOPG (Supporting Information) with a band at around 3 eV assigned to the 2p-π states and broad overlapping bands at ~5 and 8 eV associated with the 2p-σ states. The SC-SWNT film with deposited Cr (1 nm, e-beam) initially exhibited a spectrum very similar to the pristine films presumably due to the chromium oxidation that occurs upon air exposure during transfer from the e-beam to the XPS chamber and this interpretation is supported by the core Cr 2p spectrum (Figure 6c), which shows that the majority of the surface Cr is present in oxide form. To remove oxygen from the surface, the sample was sputter etched with an Ar^+ beam for 10 s; this resulted in the development of a well-defined peak at ~2.4 eV, accompanied by a shoulder at ~3.5 eV (Figure 6a). Increasing the sputtering time to 30 s did not change the position of the peak but led to a slight increase of the density of state (DOS) near the Fermi energy (E_F). The high DOS at the Fermi edge suggests that part of the surface chromium retains its metallic nature; the formation of small Cr clusters has been observed in (η^6-SWNT)$Cr_x(CO)_y$ synthesized in solution[56] and on e-beam deposition on graphene.[57]

A comparison of the photoemission spectrum of Cr/SC-SWNT with that of Cr film (prepared by e-beam deposition, sputtered with Ar^+ beam for 10 s to remove surface contamination prior to the measurement) is shown in Figure 6a. In our experiments, the Cr 3d states of the Cr film give a broad peak centered at ~1.9 eV, and thus, the peak at 2.4 eV in the Cr/SC-SWNT is related to the complexation of chromium atoms with the benzenoid ring system of the carbon nanotube surface. This agrees with previous reports, in which the d-states in metal clusters have been shown to shift to higher binding energies due to rehybridization with the graphite π^*-states.[58] The SWNT C 1s core level spectra (Figure 6b) broaden after the deposition of Cr in agreement with previous studies on the interaction of low coverages of Cr with C_{60} films[59] as a result of the hybridization of the Cr dπ orbitals with the SWNT carbon π-orbitals.

Figure 7 shows the important role of the (η^6-SWNT)Cr(η^6-SWNT) junctions in modulating the conductivity of SWNT films in the vicinity of the percolation threshold and highlights the differences in the magnitude of the response of SC-SWNT and MT-SWNT films to this phenomenon. The results clearly demonstrate that covalent bonding, in the form of the organometallic bis-hexahapto-bond (Figure 3), offers an interesting alternative to the standard approach, whereby the

dx.doi.org/10.1021/nl501212u | Nano Lett. 2014, 14, 3930–3937

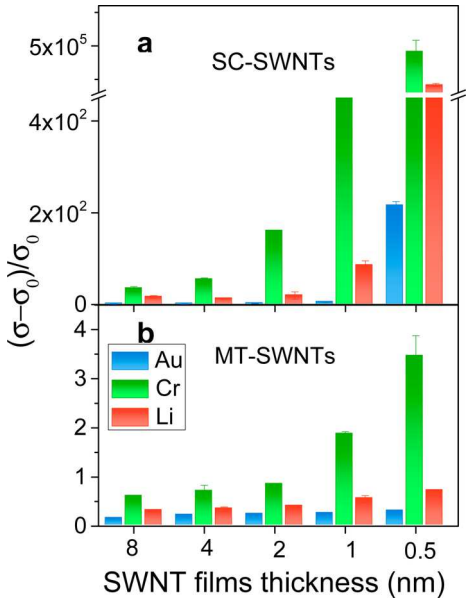

Figure 7. Conductivity enhancements at 0.1 monolayer of deposited metal for semiconducting (a) and metallic (b) SWNT films.

carrier concentration of the SWNT film is increased by chemical doping or gating.[60−62]

This variant of covalent chemistry also contrasts with the standard carbon−carbon bond forming reactions where the graphene surface carbon atoms undergo full rehybridization from sp^2 to sp^3 and in which the pyramidalization angle formally changes from $\theta_p = 0°$ to $\theta_p = 19.5°$.[4,63,64] It is important to note that the hexahapto-metal bond forms with very little *structural rehybridization*—even in the case of bis(benzene)chromium, where the attached atoms are unconstrained, the pyramidalization angle only reaches $\theta_p = 1.7°$.[4,50] In situations where the complexed carbon atoms are incorporated in a graphene surface the structural rehybridization will be even less due to the geometrical constraints of the lattice. Although it is well known that the graphene carbon atoms strongly hybridize with some transition metals, in hexahapto-coordination this electronic conjugation is able to function without marked structural rehybridization (pyramidalization).[3] The absence of structural rehybridization in bis-hexahapto-metal organometallic complexes also explains why this bond is likely the only covalent bond that can be successful in the electronic conjugation of graphene surfaces: if there is strong structural rehybridization of the reacting graphene carbon atoms, the one-center 2s, 2p orbital hybrids remain orthogonal, $\sigma-\pi$ separation is maintained and conjugation is minimized.[65] The bis-hexahapto-metal bond, which involves 12 carbon atoms coordinated with one metal atom, is highly delocalized and does not dominate the bonding of any single carbon atom and thus the individual carbon atoms maintain their conjugation with the graphene sheet—the metal d-orbitals and the carbon π-orbitals remain nonorthogonal, overlap effectively, and thereby seamlessly conjugate the two graphene sheets.

In summary, we studied the formation of covalent hexahapto (η^6) bonds of chromium atoms with the benzenoid rings of single-walled carbon nanotube films in the vicinity of the percolation threshold. The deposition of submonolayer amounts of chromium on the SWNT networks significantly increases the film conductivity as a result of reduced internanotube junction resistance. Raman and NIR spectroscopies indicate that the interaction between the transition metal and the SWNTs does not induce significant charge transfer, thereby supporting the covalent nature of the bond in agreement with the valence band structure seen in the UPS experiments.

■ ASSOCIATED CONTENT

Supporting Information

Methods, conductivity enhancements for an extended set of semiconducting SWNT films, and UPS for HOPG. This material is available free of charge via the Internet at http://pubs.acs.org.

■ AUTHOR INFORMATION

Corresponding Author

*haddon@ucr.edu.

Notes

The authors declare no competing financial interest.

■ ACKNOWLEDGMENTS

The study of the deposition of metals on carbon nanotubes was supported by NSF under contract DMR-1305724. The carbon nanotube thin film preparation was sponsored by the Defense Microelectronics Activity (DMEA) under agreement number H94003-10-2-1003. The United States Government is authorized to reproduce and distribute reprints for Government purposes, notwithstanding any copyright notation thereon. The electrical resistance data was collected in an e-beam evaporator at the CNSE Nanofabrication Center, University of California at Riverside. The SEM imaging was performed at CFAMM—UCR. XPS measurements were recorded with support from the National Science Foundation under Grant DMR-0958796. M.L.M. acknowledges support through the U.S. Department of Education GAANN award P200A120170. J.R. acknowledges support from the U.S. Department of Education under HSI-STEM undergraduate research program, award P031C110131.

■ REFERENCES

(1) Banerjee, S.; Hemraj-Benny, T.; Wong, S. S. *Adv. Mater.* **2005**, *17*, 17−29.
(2) Chan, K. T.; Neaton, J. B.; Cohen, M. L. *Phys. Rev. B: Condens. Matter Mater. Phys.* **2008**, *77*, 235430.
(3) Liu, X.; Wang, C. Z.; Hupalo, M.; Lin, H. Q.; Ho, K. M.; Tringides, M. C. *Crystals* **2013**, *3*, 79−111.
(4) Bekyarova, E.; Sarkar, S.; Wang, F.; Itkis, M. E.; Kalinina, I.; Tian, X.; Haddon, R. C. *Acc. Chem. Res.* **2013**, *46*, 65−76.
(5) Sarkar, S.; Bekyarova, E.; Haddon, R. C. *Acc. Chem. Res.* **2012**, *45*, 673−682.
(6) Sarkar, S.; Niyogi, S.; Bekyarova, E.; Haddon, R. C. *Chem. Sci.* **2011**, *2*, 1326−1333.
(7) Moser, M. L.; Tian, X.; Pekker, A.; Sarkar, S.; Bekyarova, E.; Itkis, M. E.; Haddon, R. C. *Dalton Trans.* **2014**, *43*, 7379−7382.
(8) Hu, L. B.; Hecht, D. S.; Gruner, G. *Chem. Rev.* **2010**, *110*, 5790−5844.
(9) Nirmalraj, P. N.; Lyons, P. E.; De, S.; Coleman, J. N.; Boland, J. J. *Nano Lett.* **2009**, *9*, 3890−3895.
(10) Topinka, M. A.; Rowell, M. W.; Goldhaber-Gordon, D.; McGehee, M. D.; Hecht, D. S.; Gruner, G. *Nano Lett.* **2009**, *9*, 1866−1871.
(11) Lee, E. J. H.; Balasubramanian, K.; Burghard, M.; Kern, K. *Adv. Mater.* **2009**, *21*, 2720−2724.
(12) Znidarsic, A.; Kaskela, A.; Laiho, P.; Gaberscek, M.; Ohno, Y.; Nasibulin, A. G.; Kauppinen, E. I.; Hassanien, A. *J. Phys. Chem. C* **2013**, *117*, 13324−13330.

(13) Fuhrer, M. S.; Nygard, J.; Shih, L.; Forero, M.; Yoon, Y.-G.; Mazzoni, M. S. C.; Choi, H. J.; Ihm, J.; Louie, S. G.; Zettl, A.; McEuen, P. L. *Science* **2000**, *288*, 494−497.
(14) Kim, D.; Huang, J.; Shin, H. K.; Roy, S.; Choi, W. *Nano Lett.* **2006**, *6*, 2821−2825.
(15) Zhang, H.; Bekyarova, E.; Huang, J.-W.; Zhao, Z.; Bao, W.; Wang, F.; Haddon, R. C.; Lau, C. N. *Nano Lett.* **2011**, *11*, 4047−4051.
(16) Sarkar, S.; Zhang, H.; Huang, J. W.; Wang, F.; Bekyarova, E.; Lau, C. N.; Haddon, R. C. *Adv. Mater.* **2013**, *25*, 1131−1136.
(17) Gruner, G. *J. Mater. Chem.* **2006**, *16*, 3533−3539.
(18) Kang, S. J.; Kocabas, C.; Ozel, T.; Shim, M.; Pimparkar, N.; Alam, M. A.; Rotkin, S. V.; Rogers, J. A. *Nat. Nanotechnol.* **2007**, *2*, 230.
(19) Bekyarova, E.; Ni, Y.; Malarkey, E. B.; Montana, V.; McWilliams, J. L.; Haddon, R. C.; Parpura, V. *J. Biomed. Nanotechnol.* **2005**, *1*, 3−17.
(20) Snow, E. S.; Perkins, F. K.; Houser, E. J.; Badescu, S. C.; Reinecke, T. L. *Science* **2005**, *307*, 1942−1945.
(21) Ding, M. N.; Tang, Y. F.; Gou, P. P.; Reber, M. J.; Star, A. *Adv. Mater.* **2011**, *23*, 536−540.
(22) Itkis, M. E.; Borondics, F.; Yu, A.; Haddon, R. C. *Science* **2006**, *312*, 413−416.
(23) Lu, R. T.; Li, Z. Z.; Xu, G. W.; Wu, J. Z. *Appl. Phys. Lett.* **2009**, *94*, 163110.
(24) St-Antoine, B. C.; Menard, D.; Martel, R. *Nano Lett.* **2011**, *11*, 609−613.
(25) Wu, Z.; Chen, Z.; Du, X.; Logan, J. M.; Sippel, J.; Nikolou, M.; Kamaras, K.; Reynolds, J. R.; Tanner, D. B.; Hebard, A. F.; Rinzler, A. G. *Science* **2004**, *305*, 1273−1276.
(26) Kaempgen, M.; Duesberg, G. S.; Roth, S. *Appl. Surf. Sci.* **2005**, *252*, 425−429.
(27) Zhang, D.; Ryu, K.; Liu, X.; Polikarpov, E.; Ly, J.; Tompson, M. E.; Zhou, C. *Nano Lett.* **2006**, *6*, 1880−1886.
(28) De, S.; King, P. J.; Lyons, P. E.; Khan, U.; Coleman, J. N. *ACS Nano* **2010**, *4*, 7064.
(29) McCarthy, M. A.; Liu, B.; Donoghue, E. P.; Kravchenko, I.; Kim, D. Y.; So, F.; Rinzler, A. G. *Science* **2011**, *332*, 570−573.
(30) Gwinner, M. C.; Jakubka, F.; Gannot, F.; Sirringhaus, H.; Zaumseil, J. *ACS Nano* **2012**, *6*, 539−548.
(31) Wang, F.; Itkis, M. E.; Bekyarova, E.; Haddon, R. C. *Nat. Photonics* **2013**, *7*, 459−465.
(32) Wang, F.; Itkis, M. E.; Bekyarova, E.; Tian, X.; Sarkar, S.; Pekker, A.; Kalinina, I.; Moser, M.; Haddon, R. C. *Appl. Phys. Lett.* **2012**, *100*, 223111.
(33) Timms, P. L. *Chem. Commun.* **1969**, 1033.
(34) Cloke, F. G. N. *Chem. Soc. Rev.* **1993**, *22*, 17−24.
(35) Arnold, P. A.; Petrukhina, M. A.; Bochenov, V. E.; Shabatina, T. I.; Zagorskii, V. V.; Sergeev, G. B.; Cloke, F. G. N. *J. Organomet. Chem.* **2003**, *688*, 49−55.
(36) Doherty, E. M.; S, D.; Lyons, P. E.; Shmeliov, A.; Nirmalraj, P. N.; Scardaci, V.; Joimel, J.; Blau, W. J.; Boland, J. J.; Coleman, J. N. *Carbon* **2009**, *47*, 2466−2473.
(37) Scardaci, V.; Coull, R.; Coleman, J. N. *Appl. Phys. Lett.* **2010**, *97*, 023114.
(38) Collins, P. G.; Bradley, K.; Ishigami, M.; Zettl, A. *Science* **2000**, *287*, 1801−1804.
(39) Stauffer, D. *Introduction to Percolation Theory*; Taylor & Francis: London and Philadelphia, 1985.
(40) Balberg, I.; Azulay, D.; Toker, D.; Millo, O. *Int. J. Mod. Phys. B* **2004**, *18*, 2091−2121.
(41) Bekyarova, E.; Itkis, M. E.; Cabrera, N.; Zhao, B.; Yu, A.; Gao, J.; Haddon, R. C. *J. Am. Chem. Soc.* **2005**, *127*, 5990−5995.
(42) Ural, A.; Behnam, A.; Johnson, J.; Choi, Y. *Proc. of SPIE* **2007**, *6769*, 67690B−1.
(43) Bauhofer, W.; Kovacs, J. Z. *Compos. Sci. Technol.* **2009**, *69*, 1486−1498.
(44) Kogut, P. M.; Straley, J. P. *J. Phys. C: Solid State Phys.* **1979**, *12*, 1−8.
(45) Balberg, I. *Phys. Rev. Lett.* **1987**, *59*, 1305−1308.
(46) Dresselhaus, M. S.; Dresselhaus, G. Intercalation compounds of graphite. *Advanced Physics*; Martin, D. H., Ed.; Taylor & Francis Ltd: London, 1981; Vol. *30*, pp 139−326.
(47) Haddon, R. C. *Acc. Chem. Res.* **1992**, *25*, 127.
(48) Lee, R. S.; Kim, H. J.; Fischer, J. E.; Thess, A.; Smalley, R. E. *Nature* **1997**, *388*, 255−257.
(49) Wang, F.; Itkis, M. E.; Bekyarova, E.; Sarkar, S.; Tian, X.; Haddon, R. C. *J. Phys. Org. Chem.* **2012**, *25*, 607−610.
(50) Haaland, A. *Acta Chem. Scand.* **1965**, *19*, 4146.
(51) Thess, A.; Lee, R.; Nikolaev, P.; Dai, H.; Petit, P.; Robert, J.; Xu, C.; Lee, Y. H.; Kim, S. G.; Rinzler, A. G.; Colbert, D. T.; Scuseria, G. E.; Tomanek, D.; Fischer, J. E.; Smalley, R. E. *Science* **1996**, *273*, 483−487.
(52) Elschenbroich, C. *Organometallics*, 3rd ed.; Wiley-VCH: Weinheim, 2006.
(53) Pekker, A.; Kamaras, K. *Phys. Rev. B: Condens. Matter Mater. Phys.* **2011**, *84*, 075475.
(54) Pichler, T.; Liu, X.; Knupfer, M.; Fink, J. *New J. Phys.* **2003**, *5*, 156.
(55) Das, A.; Sood, A. K. *Phys. Rev. B: Condens. Matter Mater. Phys.* **2009**, *79*, 235429.
(56) Kalinina, I.; Bekyarova, E.; Wang, Q.; Al-Hadeethi, Y. F.; Zhang, X. J.; Al-Agel, F.; Al-Marzouki, F.; Yaghmour, S.; Haddon, R. C. *Fullerenes, Nanotubes, Carbon Nanostruct.* **2014**, *22*, 47−53.
(57) Zan, R.; Bangert, U.; Ramasse, Q.; Novoselov, K. S. *Nano Lett.* **2011**, *11*, 1087−1092.
(58) Di Nardo, S.; Lozzi, L.; Passacantando, M.; Picozzi, P.; Santucci, S.; De Crescenzi, M. *Surf. Sci.* **1994**, *307*, 922−926.
(59) Ohno, T. R.; Chen, Y.; Harvey, S. E.; Kroll, G. H.; Benning, P. J.; Weaver, J. H.; Chibante, L. P. F.; Smalley, R. E. *Phys. Rev. B: Condens. Matter Mater. Phys.* **1993**, *47*, 2389−2393.
(60) Avdoshenko, S. M.; Ioffe, I. N.; Cuniberti, G.; Dunsch, L.; Popov, A. A. *ACS Nano* **2011**, *5*, 9939−9949.
(61) Li, E. Y.; Marzari, N. *ACS Nano* **2011**, *5*, 9726−9736.
(62) Dai, J.; Zhao, Y.; Wu, X.; Zeng, X. C.; Yang, J. *J. Phys. Chem. C* **2013**, *117*, 22156−22161.
(63) Niyogi, S.; Hamon, M. A.; Hu, H.; Zhao, B.; Bhowmik, P.; Sen, R.; Itkis, M. E.; Haddon, R. C. *Acc. Chem. Res.* **2002**, *35*, 1105−1113.
(64) Hu, H.; Zhao, B.; Hamon, M. A.; Kamaras, K.; Itkis, M. E.; Haddon, R. C. *J. Am. Chem. Soc.* **2003**, *125*, 14893−14900.
(65) Haddon, R. C. *Acc. Chem. Res.* **1988**, *21*, 243−249.